ENVIRONMENTAL RESEARCH
LETTERS

LETTER • OPEN ACCESS

Inverse modeling of NH_3 sources using CrIS remote sensing measurements

To cite this article: Hansen Cao *et al* 2020 *Environ. Res. Lett.* **15** 104082

Environmental Research Letters

Inverse modeling of NH_3 sources using CrIS remote sensing measurements

Hansen Cao[1], Daven K Henze[1], Mark W Shephard[2], Enrico Dammers[2,10], Karen Cady-Pereira[3], Matthew Alvarado[3], Chantelle Lonsdale[3], Gan Luo[4], Fangqun Yu[4], Liye Zhu[5,6,7], Camille G Danielson[8] and Eric S Edgerton[9]

[1] University of Colorado Boulder, Boulder, United States of America
[2] Environment Canada, Toronto, Ontario, Canada
[3] Atmospheric and Environmental Research Inc., United States of America
[4] University at Albany, New York, United States of America
[5] School of Atmospheric Sciences, Sun Yat-sen University, Guangzhou 510275, People's Republic of China
[6] Southern Marine Science and Engineering Guangdong Laboratory (Zhuhai), Zhuhai 519082, People's Republic of China
[7] Guangdong Province Key Laboratory for Climate Change and Natural Disaster Studies, Sun Yat-sen University, Guangzhou 510275, People's Republic of China
[8] Wisconsin State Laboratory of Hygiene, University of Wisconsin-Madison, Madison, United States of America
[9] Atmospheric Research & Analysis, Inc., Cary, NC, United States of America

OPEN ACCESS

RECEIVED
7 May 2020

REVISED
13 August 2020

ACCEPTED FOR PUBLICATION
7 September 2020

PUBLISHED
14 October 2020

Keywords: CrIS NH_3, 4D-Var inversion, NH_3 emissions

Supplementary material for this article is available online

Abstract

Spatiotemporal uncertainty in NH_3 emissions in the US hinders prediction of environmental effects of atmospheric NH_3. We conducted 4D-Var inversions using CrIS remote-sensing observations and GEOS-Chem to estimate monthly NH_3 emissions over the contiguous US at the $0.25^\circ \times 0.3125^\circ$ resolution in 2014, finding they are 33% higher than the prior emissions which likely underestimated most agricultural emissions, especially intense springtime fertilizer and livestock sources over the Central US. However, decreases were found in the Central Valley, southern Minnesota, northern Iowa and southeastern North Carolina during warm months. These updates increased the correlation coefficient between modeled monthly mean NH_3 and surface observations from 0.53 to 0.84, and reduced the normalized mean bias of annual mean simulated NH_3 and wet NH_4^+ by a factor of 1.3 to 12.7. Our satellite-based inversion approach thus holds promise for improving estimates of $PM_{2.5}$ and reactive nitrogen deposition throughout the world where NH_3 measurements are scarce.

1. Introduction

As the primary alkaline gas in the atmosphere, ammonia (NH_3) is an important precursor to fine particulate matter ($PM_{2.5}$), and it has effects on soil acidification, ecosystem stability, aerosol acidity, and climate change (Krupa 2003, Myhre *et al* 2009, Behera *et al* 2013, Nah *et al* 2018, Sutton *et al* 2011). NH_3 emissions are a key factor in $PM_{2.5}$ formation and its reduction has been reported as a cost-effective way to mitigate air pollution (Pinder *et al* 2007, Wu *et al* 2016). Additionally, as the increasingly dominant form of reactive nitrogen (Nr) (Du *et al* 2014, Ellis *et al* 2013, Li *et al* 2016), NH_3 plays a significant role in excessive NH_3 and NH_4^+ deposition that can harm regional eco-biodiversity through eutrophication and acidification (Erisman *et al* 2013). To better understand and mitigate the environmental effects of NH_3, accurate and up-to-date NH_3 emission estimates are required.

Agricultural emissions are the main source of atmospheric NH_3 at national scales (Huang *et al* 2012, EEA 2017, U.S. EPA 2018), although locally non-agricultural sources can dominate (Felix *et al* 2014, Fenn *et al* 2018, Berner *et al* 2020). In the US, agricultural practices (livestock and fertilizer use) account for ~ 80% of national NH_3 emissions, followed by biomass burning, transportation, industrial activities, residential activities, and other emissions (U.S. EPA 2018). Table 1 shows anthropogenic NH_3 emission inventories for the contiguous US in 2005 to 2014 ranging from 2.4 to 3.40 Tg N a^{-1} (European CommissionEuropean Commission

[10] Current address: TNO, Department of Climate, Air and Sustainability, Utrecht, The Netherlands.

2011, Paulot *et al* 2014, Janssens-Maenhout *et al* 2015, Crippa *et al* 2018, Hoesly *et al* 2018). This large uncertainty in NH_3 emission inventories is due to scarce measurements of locally representative emission factors and out-of-date activity data (Beusen *et al* 2008, Holt *et al* 2017).

Alternatively, observations of NH_3 and its reaction products (i.e. NH_4^+) can provide top-down constraints on NH_3 sources. In-situ wet deposition measurements were first used to constrain the seasonal cycle and magnitude of US NH_3 emissions by Gilliland *et al* (2003), which inspired similar subsequent studies (Pinder *et al* 2006, Henze *et al* 2009, Zhang *et al* 2012, Paulot *et al* 2014). Challenges with these approaches are limited in-situ observations and model uncertainties in precipitation and aerosol formation.

Satellite-based NH_3 observations can provide timely and spatially comprehensive constraints on NH_3 sources (Zhu *et al* 2013, Schiferl *et al* 2016, Zhang *et al* 2018, Van Damme *et al* 2018, Dammers *et al* 2019, Clarisse *et al* 2019). Atmospheric NH_3 is monitored from space by infrared spectrometers onboard the satellites TES, IASI, AIRS and CrIS (Shephard *et al* 2011, Van Damme *et al* 2014, Warner *et al* 2016, Shephard *et al* 2015). Zhu *et al* (2013) and Zhang *et al* (2018) derived NH_3 emissions from TES NH_3 observations for the globe and China, respectively, and found that bottom-up inventories generally underestimated agricultural NH_3 emissions during warm months. Schiferl *et al* (2016) used summertime IASI NH_3 columns to constrain interannual variability of modeled NH_3 over the contiguous US and explored the drivers of interannual variability. Most recently, Van Damme *et al* (2018) and Dammers *et al* (2019) derived NH_3 emissions from large point-sources using IASI and CrIS observations via a relationship between lifetime, atmospheric column concentrations and emissions, finding that the HTAP v2 inventory underestimates NH_3 emissions from large point-sources over North America by a factor of 2.9 (Dammers *et al* 2019). To accurately estimate high-resolution gridded NH_3 emissions using CrIS in an inversion, Li *et al* (2019) showed using pseudo observations that 4D-Var methods are needed to capture the impact of transport and the spatially variable role of HNO_3 and H_2SO_4 on NH_3 lifetime. Thus, variability or uncertainty in NO_x and SO_2 emissions needs to be accounted for in top-down estimates of NH_3 emissions (Yu *et al* 2018, Liu *et al* 2018).

Here we conduct the first 4D-Var inversions with CrIS NH_3 observations. Here we focus on 2014, as this is the first period for which a complete year of CrIS NH_3 retrievals were available. We use daytime CrIS NH_3 vertical profiles with GEOS-Chem and its adjoint (Henze *et al* 2007) to estimate gridded monthly NH_3 emissions over the contiguous US in 2014. CrIS NH_3 combines extensive spatial coverage, low noise and fine spatial resolution (Shephard *et al* 2015); it has greater spatial coverage than TES, with global coverage similar to IASI and AIRS, and lower signal noise compared to other sensors (Zavyalov *et al* 2013), which improves sensitivity in the boundary layer. Our CrIS-derived NH_3 emissions are evaluated using surface NH_3 measurements from the AMoN (http://nadp.sws.uiuc.edu/AMoN/) and SEARCH (Hansen *et al* 2003) networks, and NH_4^+ wet deposition measurements from the NADP network (http://nadp.slh.wisc.edu/ntn/) in 2014.

2. CrIS NH_3 observations

CrIS is an infrared sounder onboard the Sun-synchronous satellite Suomi National Polar-orbiting Partnership (SNPP) (Tobin 2012) launched in October 2011 (used in this study) and the NOAA-20 launched in November 2017 (Glumb *et al* 2018). The first CrIS has a cross-track scanning swath width of 2200 km and a nadir spatial resolution of 14 km, which enables CrIS to achieves global coverage twice a day with daytime and nighttime overpasses at 13:30 local time (LT) and at 01:30 LT, respectively. NH_3 profile observations are retrieved through the CrIS Fast Physical Retrieval algorithm (CFPR), which minimizes the difference between measured and simulated spectral radiance in the NH_3 spectral feature around 967 cm^{-1} (Shephard *et al* 2015). The CFPR algorithm uses three *a priori* NH_3 profiles, representative of polluted, moderately polluted, and clear conditions. For each NH_3 retrieval, one *a priori* profile is selected based on estimated NH_3 signal (Shephard *et al* 2015). Pixel-specific *a priori* profiles and averaging kernels comprise the observation operator ($\boldsymbol{H}$), which is essential for comparison between satellite retrievals and model simulations. We used high-quality (QF = 5) daytime CrIS v1.5 NH_3 observations (Shephard *et al* 2020) over the North America domain [127°-65°W, 22°-57°N]. Daytime CrIS NH_3 observations have been validated by and show good agreement with ground-based and aircraft observations collected in select regions (Shephard *et al* 2015, Dammers *et al* 2017).

Figure 1 shows the spatial and seasonal variability of CrIS surface NH_3 concentrations in 2014. Higher NH_3 concentrations are found in warmer months over agricultural areas (like the central US, the Central Valley, southeastern Washington and southern Idaho), consistent with AIRS-based analysis of Warner *et al* (2017). CrIS detects a springtime peak over the north central US (South Dakota, Nebraska, western Iowa, northern Kansas), which is also detected by AIRS in March during 2014 to 2016 (Warner *et al* 2017) and is mainly caused by enhanced emissions from intense fertilizer use (Cao *et al* 2018), followed by minor contributions from temperature-driven increases in emissions. In contrast, summertime peaks over the Central Valley, the

Table 1. NH_3 emission estimates (Tg N a^{-1}) for the contiguous US.

Literature	Target year	Anthropogenic NH_3 emissions
Bottom-up		
NEI2008	2006	3.1
Paulot *et al* (2014)	2005-2008	2.4[a]
EDGAR v4.2	2008	2.9
EDGAR v4.3.2	2010	3.40[c]
HTAP v2	2010	2.95
CEDS_2018	2014	3.05
Top-down		
Zhang *et al* (2012)	2006-2008	2.3
Paulot *et al* (2014)	2005-2008	2.8[b]
Dammers2019	2013-2017	1.07[d] (2.9 times HTAP v2)
This study	2014	3.91

[a]Bottom-up anthropogenic NH_3 emissions, with agricultural emissions taken from MASAGE inventory.
[b]Total NH_3 emission (anthropogenic + biomass burning + natural sources) estimate derived from NADP wet NH_4^+ deposition measurements.
[c]Including NH_3 emissions from agricultural soils (AGS), agricultural waste burning (AWB), manure management (MNM), chemical processes (CHE), power industry (ENE), combustion for manufacturing (IND), non-metallic minerals production (NMM), energy for buildings (RCO), oil refineries and transformation industry (REF_TRF), solid waste incineration (SWD_INC), solid waste landfills (SWD_LDf), shipping (TNR_Ship), railways,pipelines, off-road transport (TNR_Other), Road transportation (TRO), waste water handling (WWT) (Crippa *et al* 2018).
[d]Only NH_3 emissions from 48 large point-sources (mainly industrial and agricultural sources) over North America.

south central US (North Texas and western Kansas), southeastern Washington and southern Idaho are likely caused by temperature-driven increases in emission factors of both livestock and fertilizer (Mikkelsen *et al* 2009, McQuilling and Adams 2015).

3. GEOS-Chem adjoint and 4D-Var inversion

The GEOS-Chem adjoint v35m, which is based on v8 of the forward model with updates through v9, is driven by Goddard Earth Observing System (GEOS-FP) assimilated meteorological fields with a horizontal resolution of 0.25° latitude × 0.312 5° longitude and 47 vertical levels over a domain of 127°-65°W and 22°-57°N. Global 2° latitude × 2.5° longitude simulations are used for boundary conditions.

As NH_x is not directly involved in other gas-phase chemical reactions in GEOS-Chem (hereinafter referred to as GC), we construct an offline NH_x simulation to reduce the computational cost of 4D-Var inversion at high resolution (0.25° latitude × 0.312 5° longitude) following Paulot *et al* (2014) and Zhang *et al* (2018). This simulation includes emissions, wet deposition (Liu *et al* 2001, Wang *et al* 2011, Amos et al 2012) and dry deposition (Wesely 1989, Wang *et al* 1998, Zhang *et al* 2001), transport of NH_3 and NH_4^+, and NH_x partitioning (Binkowski and Roselle 2003, Park *et al* 2004) driven by archived hourly SO_4^{2-}, HNO_3, and NO_3^- concentrations from the standard O_3-NO_x-VOC-aerosol simulation (hereinafter referred to as fullchem). We reduce the simulated high-biased HNO_3 (Zhang *et al* 2012, Heald *et al* 2012) by 15% at each time step (10 minutes) following Heald *et al* (2012). The difference between monthly mean offline-simulated surface NH_3 and fullchem-simulated surface NH_3 in July is within 0.1% across the contiguous US.

We used NH_3 emissions in 2010 from HTAP v2 (Janssens-Maenhout *et al* 2015) as the prior anthropogenic emissions for global and regional simulations. NH_3 emissions for the contiguous US in HTAP v2 are from the NEI2008 emission inventory, on the lower end (2.95 Tg N a^{-1}) of the range of previous estimates (table 1). No significant trend is found in NH_3 emissions from 2010 to 2014 in the US (Butler *et al* 2016). Changes in emissions of SO_x and NO_x can affect NH_3 column concentrations (Liu *et al* 2018, Yu *et al* 2018). Here we reduce SO_2 and NO_x emissions over the US from HTAP v2 (originally for the year 2010) by 37.6% and 15.1%, respectively, as the emissions for the year 2014, according to EPA-based emission trends from 2010 to 2014 (Yu *et al* 2018).

Diurnal variability in NH_3 emissions and concentrations is a potential source of uncertainty in satellite-based emission estimates Dammers *et al* (2019) since there is only a single daytime overpass (13:30 LT for CrIS). We thus updated the standard GC simulation (driven by static monthly emissions, referred to as the GC default) to include diurnal variability of livestock NH_3 emissions following Zhu *et al* (2015), which enables GC (referred to as GC prior) to better reproduce the diurnal variability of the hourly surface NH_3 measurements from SEARCH (figure S1).

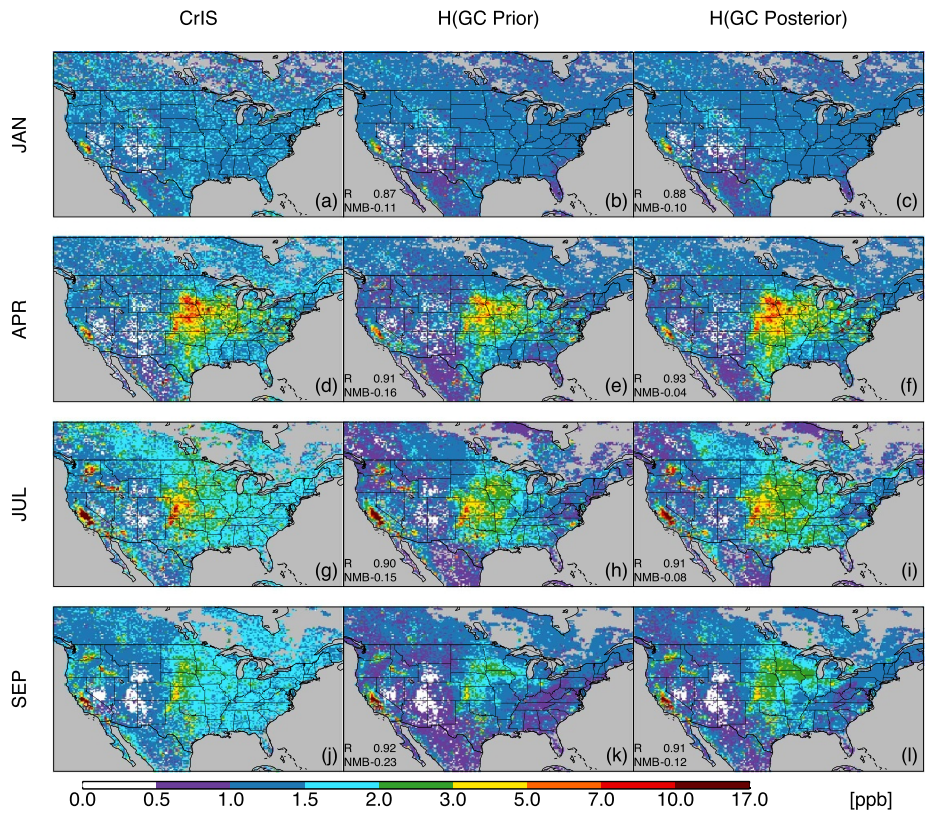

Figure 1. Monthly mean surface NH_3 concentrations from CrIS((a), (d), (g), (j)), simulation driven by prior emissions ((b), (e), (h), (k)), simulation driven by posterior emissions ((c), (f), (i), (l)), respectively, in January, April, July, and September in 2014.

We apply this updated GC model and its adjoint (Henze *et al* 2007) to our 4D-Var inversion, which iteratively minimizes the cost function J:

$$J = \gamma(\boldsymbol{x}-\boldsymbol{x_a})^T\boldsymbol{S_a^{-1}}(\boldsymbol{x}-\boldsymbol{x_a}) + (\boldsymbol{H(x)}-\boldsymbol{y_o})^T\boldsymbol{S_o^{-1}}(\boldsymbol{H(x)}-\boldsymbol{y_o}), \quad (1)$$

J is the mismatch between the observations ($\boldsymbol{y_o}$) and the model ($\boldsymbol{H(x)}$) plus the deviation of adjusted emission scaling factors ($\boldsymbol{x}$, the ratio of adjusted emissions to prior emissions) from their initial values ($\boldsymbol{x_a}$). $\boldsymbol{S_o}$ is the observation error covariance matrix from the CrIS v1.5 retrieval product. Here we apply the CrIS linear averaging kernel (derived from the CrIS logarithmic averaging kernel) to the model simulation to convert the simulated NH_3 to observation space. The lower and upper bounds of $\boldsymbol{x}$ are set to be 0.5 and 5.0, respectively. We assume the diagonal elements of the prior emission error covariance matrix ($\boldsymbol{S_a}$) are 100% and the correlation length is 100 km in latitudinal and longitudinal directions. γ is a regulation parameter introduced to balance the observation and penalty terms, determined to be 100 through an L-curve approach (Hansen *et al* 1999). The minimization of equation (1) is found iteratively using the L-BFGS-B algorithm (Byrd *et al* 1995). The optimization is considered converged when the change across iterations of the cost function is less than 10^{-4}.

4. Results

Figure 1 and table S1 (stacks.iop.org/ERL/15/104082/mmedia) compare GC surface NH_3 concentrations driven by prior and posterior emissions (hereafter referred to as GC prior and GC posterior, respectively) to surface-level concentrations from CrIS NH_3 profiles for different months of 2014. With higher concentrations found over the central US and the Central Valley in warm months, GC prior generally captures the spatial pattern (R between 0.82 to 0.94 throughout the whole year except December, see table S1) and seasonal variability of surface NH_3 observed by CrIS, but has a year-round low bias across most of the contiguous US with monthly domain NMB between -8% to -26% (table S1), indicating broad underestimation of emissions in the prior inventory. Meanwhile, high biases are found over the Central Valley, South Minnesota and North Iowa, as well as southeast North Carolina during warm months. Compared to GC prior, GC posterior better reproduces the magnitude, seasonality, and spatial variability in surface NH_3 concentration from the CrIS profiles across most of the domain (especially over the central US during warmer months), with slightly improved R and significantly decreased NMB (between -0.02 to -0.12, see table S1) during most of the year, with the exception of November, December and January likely owing

to smaller satellite instrument sensitivity to smaller surface concentrations in cold months. GC posterior also reduced the gap between modeled and observed vertical profiles most notably during warm months (figure S2) compared to GC prior.

Figures 2(a) and (b) show the prior and posterior annual anthropogenic NH_3 emissions, respectively. They have similar spatial patterns, but the posterior emissions are 33% higher than the prior annual emissions. Figure 2(c) shows increases across most of the contiguous US, especially over the central and northwest US (dominated by concentrated livestock operations and crop farming), while there were small-scale decreases (< 40%) in the Central Valley, South Minnesota and North Iowa, as well as southeast North Carolina.

Figure 2(d) shows that total posterior anthropogenic NH_3 emissions peak in summer and have a similar seasonal pattern as the prior emissions, but increased significantly throughout the whole year by a factor of 1.1 to 1.6, especially during warm months, despite small-scale decreases (figure S3) in the Central Valley and southeast North Carolina, as well as in Northwest Iowa and southwest Minnesota from March to October. The largest percentage increase (about 64%) was found in May, strongly suggesting large underestimates in agricultural activities and emission factors.

Combining spatial distributions of NH_3 emission from different animal types based on Carnegie Mellon University's livestock emission model (U.S. EPA 2018) and spatial and temporal distribution of fertilizer application rate from Cao *et al* (2018), as well as figure 2(c) and figure S3, we can roughly conclude which sources of NH_3 emissions might be biased in the prior inventory. The substantial underestimates over the central US (South Dakota, Nebraska, southwestern Kansas, northern Texas, and southern Wisconsin) and the northwestern US in spring are most likely due to underestimate of fertilizer use and manure application. The underestimate in northeastern Colorado and northern Texas during most of the year is likely caused by underestimated cattle emissions, consistent with previous studies (Battye *et al* 2016, Kille *et al* 2017) based on aircraft, ground, and satellite measurements. The moderate underestimate over most of the southeastern US is more likely due to poultry emissions, whereas the underestimate over southeastern North Carolina is more likely due to swine emissions. For southeastern Pennsylvania, the underestimate might be due to an underestimate of both livestock (swine and poultry) and fertilizer emissions during warm months. For the Delmarva peninsula area, the year-round underestimate is more likely caused by low emission factors of broiler chicken emissions (Russ and Schaeffer 2017).

While increases in NH_3 emissions occur over most of the domain, persistent decreases are found during warm months in a few areas (e.g. the Central Valley, northwest Iowa and southwest Minnesota, as well as Clinton and Duplin) with the densest cattle or swine population. These heterogeneous adjustments of NH_3 emissions might be caused by 1) biased emission factors due to lack of differentiation in animal size and age, pasture and feedlot cattle, and manure management techniques (Battye *et al* 2019), and 2) the potential underestimation of CrIS NH_3 over very high-emission areas (Dammers *et al* 2017).

Table 1 compares our posterior NH_3 emissions for the contiguous US in 2014 to previous bottom-up (European Commission 2011, Janssens-Maenhout *et al* 2015, Hoesly *et al* 2018, Crippa *et al* 2018) and top-down (Zhang *et al* 2012, Paulot *et al* 2014, Dammers *et al* 2019) studies. Our CrIS-derived annual NH_3 emission estimate is 3.91 Tg N a^{-1}, consistently higher than previous bottom-up estimates ranging from 2.4 to 3.40 Tg N a^{-1} and ground-based measurement derived estimates between 2.3 and 2.8 Tg N a^{-1}. The generally higher estimates derived from satellite observations are likely due to 1) its greater spatial coverage and detection of elevated concentrations above surface level in the NH_3 profiles, and 2) the high bias (< 5% for most values, but > 30% for small values) in CrIS NH_3 concentrations (Dammers *et al* 2017). The difference between our estimate (1.3 times higher than HTAP v2 estimate) and that also derived from CrIS by Dammers *et al* (2019) (2.9 times higher than HTAP v2 estimate), might be due to the fact that Dammers *et al* (2019) used time-constant emission profiles for large point sources, targeted the years 2013 to 2017 while we only target the year 2014 which has lower CrIS NH_3 concentrations compared to other years (Shephard *et al* 2020), used several estimated constant lifetimes (average of 2.35 h), and did not remove the influence of the CrIS retrieval *a priori* NH_3 information. With proper diurnal emission profiles, top-down estimate from Dammers *et al* (2019) could be reduced by a factor of 2.0, which is 1.45 times higher than HTAP v2 estimate and much closer to our top-down estimate (1.3 times higher than HTAP v2 estimate) (Dammers 2020). For our 4D-Var inversion, application of averaging kernels has a larger impact on top-down NH_3 emissions than diurnal variability of livestock emissions (see figure S5(a)).

Compared to previous top-down (Gilliland *et al* 2006, Henze *et al* 2009, Zhang *et al* 2012, Zhu *et al* 2013, Paulot *et al* 2014) and bottom-up (Pinder *et al* 2006, Cooter *et al* 2012, Paulot *et al* 2014, Janssens-Maenhout *et al* 2015) estimates, our posterior monthly emissions have similar summer-/winter contrast, but generally higher magnitudes during most of the year except April, May and July. Our posterior estimates for mid-late spring (April and May) and July are lower than those from Gilliland *et al* (2006) based on NADP wet NH_4^+, and Zhu *et al* (2013) based on TES NH_3, respectively. The largest difference among these monthly estimates lies in the

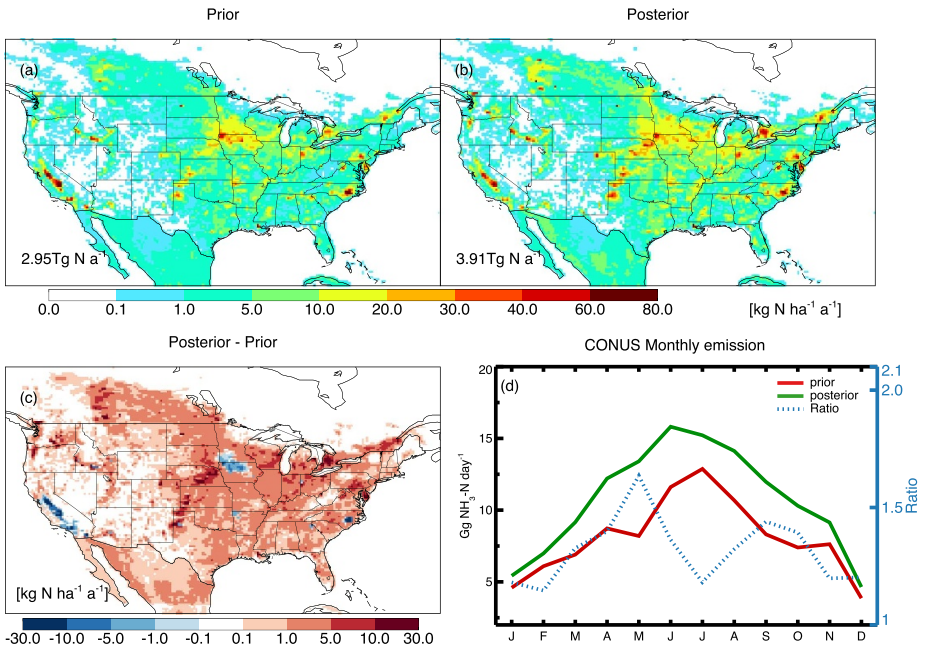

Figure 2. Spatial distribution of prior (a) and posterior (b) annual anthropogenic NH_3 emissions; (c) difference between posterior and prior annual anthropogenic NH_3 emissions; (d) prior (red solid) and posterior (green solid) monthly anthropogenic NH_3 emission for contiguous US, ratio of posterior/prior (blue dotted line).

spring/summer contrast. Wet NH_4^+-based emissions (Gilliland *et al* 2006, Pinder *et al* 2006, Paulot *et al* 2014) are generally higher in spring than in summer likely due to most of the NADP-wet NH_4^+ monitoring sites being more representative of agricultural land cover (Bigelow *et al* 2001) where fertilizer use and manure application peak in spring, while satellite NH_3-based estimates, such as Zhu *et al* (2013) and our study, are always higher in summer likely due to the satellite's more uniform spatial coverage that captures the agricultural emission increases (both in livestock and fertilizer use) driven by increasing ambient temperature throughout the domain (figures 1(d) and (g)). Meanwhile, in-situ measurement-based inversions are prone to underestimating small but widespread NH_3 emissions due to the sparsity of monitoring sites. The data filtering (retaining only pixels with Quality Flag of 5) in our inversion and the averaged 15% high bias in CrIS NH_3 retrieval over the US compared to AMoN measurements (Kharol *et al* 2018) might also contribute to our generally higher posterior NH_3 emissions, especially over the East US.

To further evaluate our CrIS-derived NH_3 emissions, we next compare prior and posterior simulated surface NH_3 and wet NH_4^+ concentrations against measurements from the AMoN, NADP, and SEARCH monitoring networks. For AMoN sites, we filtered out those sites with monthly mean beyond the monthly domain average by three times the standard deviation.

Correlation coefficients between time series of monthly mean GC surface concentrations and AMoN NH_3 measurements in 2014 for each site before and after emission optimization, respectively, are shown in figures 3(a) and (b). GC prior generally captures the spatial pattern (R between 0.51 and 0.81 throughout the whole year except February, figure S4) and seasonal variability in AMoN NH_3, but only 11 out of 65 sites had a correlation coefficient greater than 0.6. Ten sites (AZ98, FL11, GA40, GA41, MD99, NS01, NY96, OH02, SC05, WV18) have R less than -0.1. Most of these ten sites are located where NH_3 emissions are small (less than 5 kg N ha^{-1} a^{-1}, see figure 2(a)). Emission optimization enables the model to better reproduce the observed seasonal variability, increasing the number of sites with R greater than 0.6 to 30 and further leading to a moderate increase (from 0.53 to 0.84) in R between domain average monthly mean GC and AMoN measurements.

Figures 3(c) and (d) show the normalized mean bias of annual mean GC surface NH_3 relative to AMoN NH_3 measurements for each site. Low bias is found in the annual mean GC prior at most sites. 36 of 65 sites have NMB magnitude greater than 0.4. Emission optimization largely reduces the low bias for most sites at the annual scale, leading to an approximately three-fold decrease in domain NMB (from -0.45 to -0.16) at the annual scale. The number of sites with NMB magnitude greater than 0.4 is reduced to 28. Moreover, the magnitude of posterior monthly domain NMB is also reduced by a factor between 1.4 and 12.7 throughout the year except November (see figure S4).

Similar but less significant improvement is found in comparison with domain average monthly mean NADP wet deposition of NH_4^+ in 2014 (figure 3(e)). GC-simulated NH_4^+ wet deposition consists of wet

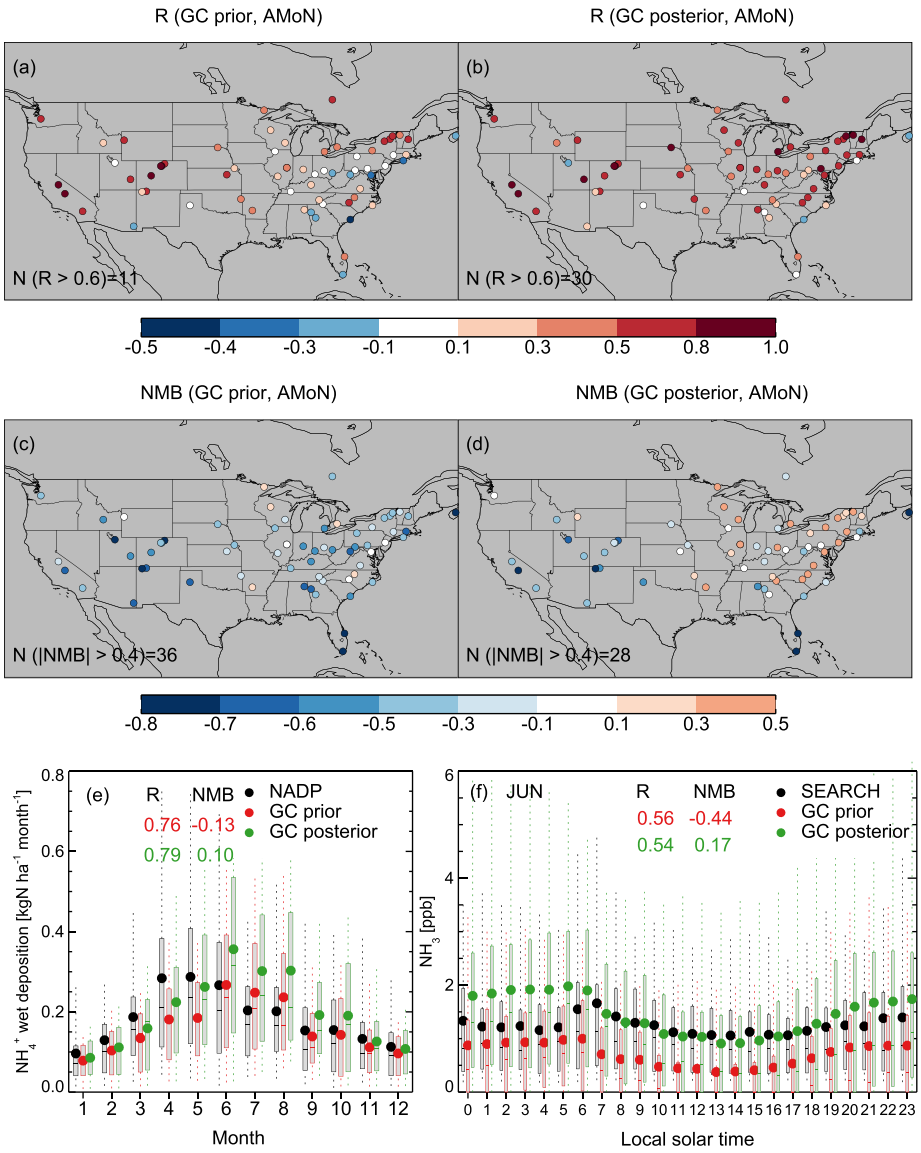

Figure 3. (a) Correlation coefficient between prior monthly mean GC surface NH_3 and monthly mean AMoN NH_3 measurements; (b) posterior correlation coefficient; (c) normalized mean bias of prior annual mean GC surface NH_3 relative to annual mean AMoN NH_3 measurements; (d) posterior normalized mean bias; (e) Boxplot of monthly mean of GC prior and GC posterior NH_4^+ wet deposition, as well as NADP NH_4^+ wet deposition; (f) Boxplot of hourly mean of GC prior and GC posterior surface NH_3, as well as SEARCH NH_3 in June.

deposition of aerosol-phase NH_4^+ and gas-phase NH_3. To remove the bias caused by the difference between measured and simulated precipitation, we scaled the measured wet NH_4^+ by the ratio of modeled and measured precipitation, NADP wet $NH_4^+ \times (P_{model}/P_{NADP})^{0.6}$, following Paulot *et al* (2014). We only compared simulated wet NH_4^+ to measurements with P_{model}/P_{NADP} between 0.25 and 4.0 (Paulot *et al* 2014). NADP-measured NH_4^+ wet deposition is higher in warm months and peaks in spring, likely due to intense fertilizer and manure application. GC prior can capture the general summer/winter contrast but underestimates the magnitude during most of the year, especially in spring. Our CrIS-derived NH_3 emissions improve the overall ability of the model to reproduce NADP wet measurements with a slight increase in *R* (from 0.76 to 0.79) and a slight decrease in NMB magnitude (from -0.13 to 0.10), although GC posterior still misses the springtime peak. The maximum percentage increase in anthropogenic emissions in the spring (figure 2(d)) is consistent with the higher springtime emissions reflected by NADP wet NH_4^+.

Figure 3(f) shows another evaluation using hourly measurements of surface NH_3 collected from five SEARCH sites (BHM, CTR, JST, OLF, YRK) in June 2014. While having a similar diurnal cycle as GC prior, GC posterior better reproduces the magnitude of monthly-averaged hourly SEARCH NH_3, reducing the NMB from −0.44 to 0.17 in June. A substantial decrease from -0.38 to 0.03 in NMB is found at the annual scale.

5. Discussion and conclusions

This study presents the first 4D-Var inversion of NH_3 using CrIS measurements. CrIS-derived monthly NH_3 emissions are higher than HTAP v2 emissions across most of the contiguous US and throughout most of the year, despite occasional small decreases ($< 40\%$), revealing a substantial underestimate of NH_3 emissions from springtime fertilizer and manure application over the central US and widespread underestimation of total agricultural NH_3 emissions (fertilizer + manure) associated with warm temperature.

New CrIS observations since 2018 (Glumb *et al* 2018) could help future studies constrain long-term NH_3 trends. We also emphasize that use of an observation operator (which contains critical information about the instrument's sensitivity to NH_3) is critical for making comparisons between model simulations and CrIS NH_3 profiles. For example, without consideration of the observation operator the difference between simulations and CrIS observations at surface level over polluted areas in July 2014 is three times higher than when using the observation operator (see figure S5 (a)), and commensurate differences could be expected in top-down emission estimates.

Given the critical role of NH_3 in $PM_{2.5}$ formation and excessive deposition of Nr, evaluation of NH_3 emission is important for environmental policy. A series of NH_3 emission control policies have been implemented in Europe (Giannakis *et al* 2019). However, NH_3 emissions in the US have not been regulated for multiple reasons, one of which is the difficulty of emission monitoring (United States Department of Agriculture 2014). Top-down NH_3 emissions at high spatial resolution ($0.25° \times 0.3125°$) derived from CrIS observations may provide future policy makers quantitative support for monitoring changes in NH_3 emissions.

Acknowledgments

This study is supported by NASA 80NSSC18K0689. We acknowledge the National Atmospheric Deposition Program (NADP) for providing surface NH_3 (available at http://nadp.slh.wisc.edu/amon/) and wet NH_4^+ measurements (available at http://nadp.slh.wisc.edu/NTN/). We acknowledge the SouthEastern Aerosol Research and Characterization Network (SEARCH) for providing hourly measurements of surface NH_3 (available at https://10.412 1/uuid:d9ac07c4-2041-4241-8635-3838c657a6ff). We thank Jesse Bash and Venkatesh Rao (U.S. EPA) for useful discussions. The CrIS CPFR Version 1.5 ammonia data for 2014 is publicly available from Environment and Climate Change Canada (ECCC) (https://hpfx.collab.science.gc.ca/mas001/satellite_ext/cris/snpp/nh3/v1_5/global/2014/). GEOS-Chem adjoint v35m source code is available online (http://wiki.seas.harvard.edu/geos-chem/index.php/GEOS-Chem_Adjoint).

ORCID iD

Hansen Cao https://orcid.org/0000-0003-2713-0430

References

Amos H M, Jacob D J, Holmes C D, Fisher J A, Wang Q, Yantosca R M and Sunderland E M 2012 Gas-particle partitioning of atmosphericHg(II) and its effect on global mercury deposition *Atmos. Chem. Phys.* **12** 591–603

Battye W H, Bray C D, Aneja V P, Tong D, Lee P and Tang Y 2016 Evaluating ammonia (NH_3) predictions in the NOAA National Air Quality Forecast Capability (NAQFC) using in situ aircraft, ground-level and satellite measurements from the DISCOVER-AQ Colorado campaign *Atmos. Environ.* **140** 342–51

Battye W H, Bray C D, Aneja V P, Tong D, Lee P and Tang Y 2019 Evaluating Ammonia (NH_3) Predictions in the NOAA NAQFC for Eastern North Carolina Using Ground Level and Satellite Measurements *J. Geophys. Res.* **124** 8242–59

Behera S N, Sharma M, Aneja V P and Balasubramanian R 2013 Ammonia in the atmosphere: a review on emission sources, atmospheric chemistry and deposition on terrestrial bodies *Environ. Sci. Pollut. Res.* **20** 8092–131

Berner A H and Felix D 2020 Investigating ammonia emissions in a coastal urban airshed using stable isotope techniques *Sci. Total Environ.* **707** 134952

Beusen A, Bouwman A, Heuberger P, Drecht G V and Hoek K V D 2008 Bottom-up uncertainty estimates of global ammonia emissions from global agricultural production systems *Atmos. Environ.* **42** 6067–77

Bigelow D S, Dossett S R and Bowersox V C 2001 Instruction manual: Nadp/ntn site selection and installation NADP Program Office, Illinois State Water Survey

Binkowski F S and Roselle S J 2003 Models-3 Community Multiscale Air Quality (CMAQ) model aerosol component 1.Model description *J. Geophys. Res.* **108** 4183

Butler T, Vermeylen F, Lehmann C, Likens G and Puchalski M 2016 Increasing ammonia concentration trends in large regions of theUSA derived from theNADP/AMoN network *Atmos. Environ.* **146** 132–40

Byrd R H, Lu P, Nocedal J and Zhu C 1995 A limited memory algorithm for bound constrained optimization *SIAM J. Sci. Comput.* **16** 1190–208

Cao P, Lu C and Yu Z 2018 Historical nitrogen fertilizer use in agricultural ecosystems of the contiguousUnited States during 1850–2015: application rate, timing and fertilizer types *Earth Syst. Sci. Data* **10** 969–84

Clarisse L, Van Damme M, Clerbaux C and Coheur P-F 2019 Tracking down global NH_3 point sources with wind-adjusted superresolution *Atmos. Meas. Tech.* **12** 5457–73

Commission E 2011 JRC/PBL, Emission Database for Global Atmospheric Research (EDGAR), release version 4.2. (http://edgar.jrc.ec.europa.eu/)

Cooter E J, Bash J O, Benson V and Ran L 2012 Linking agricultural crop management and air quality models for regional to national-scale nitrogen assessments *Biogeosciences* **9** 4023–35

Crippa M, Guizzardi D, Muntean M, Schaaf E, Dentener F, van Aardenne J A and Janssens-Maenhout G 2018 Gridded

emissions of air pollutants for the period 1970–2012 within EDGAR v4.3.2 *Earth Syst. Sci. Data* **10** 1987–2013

Dammers E 2020 Personal communication with Enrico Dammers Personal communication with Enrico Dammers

Dammers E, McLinden C A, Griffin D, Shephard M W, Van Der Graaf S, Lutsch E and Erisman J W 2019 NH_3 emissions from large point sources derived from CrIS and IASI satellite observations *Atmos. Chem. Phys.* **19** 12261–93

Dammers E, Shephard M W, Palm M, Cady-Pereira K, Capps S, Lutsch E and Erisman J W 2017 Validation of the CrIS fast physical NH_3 retrieval with ground-based FTIR *Atmos. Meas. Tech.* **10** 2645–67

Du E, de Vries W, Galloway J N, Hu X and Fang J 2014 Changes in wet nitrogen deposition in theUnited States between 1985 and 2012 *Environ. Res. Lett.* **9** 095004

EEA 2017 European Union emission inventory report 1990-2015 under the UNECE Convention on Long-range Transboundary Air Pollution (LRTAP)

Ellis R A, Jacob D J, Sulprizio M P, Zhang L, Holmes C D, Schichtel B A and Lynch J A 2013 Present and future nitrogen deposition to national parks in theUnited States: Criticalload exceedances *Atmos. Chem. Phys.* **13** 9083–95

Erisman J W, Galloway J N, Seitzinger S, Bleeker A, Dise N B, Petrescu A M R and de Vries W 2013 Consequences of human modification of the global nitrogen cycle *Philos Trans R Soc Lond B Biol Sci.* **368** 1–9

Felix J D, Elliott E M, Gish T, Maghirang R, Cambal L and Clougherty J 2014 Examining the transport of ammonia emissions across landscapes using nitrogen isotope ratios *Atmos. Environ.* **95** 563–70

Fenn M E, Bytnerowicz A, Schilling S L, Vallano D M, Zavaleta E S, Weiss S B and Hanks K 2018 On-road emissions of ammonia: An underappreciated source of atmospheric nitrogen deposition *Sci. Total Environ.* **625** 909–19

Giannakis E, Kushta J, Bruggeman A and Lelieveld J 2019 Costs and benefits of agricultural ammonia emission abatement options for compliance with European air quality regulations *Environ. Sci. Eur.* **31** 93

Gilliland A B, Appel K W, Pinder R W and Dennis R L 2006 Seasonal NH_3 emissions for the continentalUnited States: Inversemodel estimation and evaluation *Atmos. Environ.* **40** 4986–98

Gilliland A B, Dennis R L, Roselle S J and Pierce T E 2003 Seasonal NH_3 emission estimates for the easternUnited States based on ammonium wet concentrations and an inverse modeling method *J. Geophys. Res.* **108** 4477

Glumb R, Suwinski L, Wells S, Glumb A, Malloy R and Colton M 2018 The JPSS CrIS Instrument and the Evolution of Space-Based Infrared Sounders

Hansen D A, Edgerton E S, Hartsell B E, Jansen J J, Kandasamy N, Hidy G M and Blanchard C L 2003 The Southeastern Aerosol Research and Characterization Study: Part 1—Overview *J. Air Waste Manage. Assoc.* **53** 1460–71

Hansen P C 1999 The L-curve and its use in the numerical treatment of inverse problems *Computational Inverse Problems in Electrocardiology* (Southampton: WIT Press) pp 119–42

Heald C L, Collett J J L, Lee T, Benedict K B, Schwandner F M, Li Y and Pye H O T 2012 Atmospheric ammonia and particulate inorganic nitrogen over theUnited States *Atmos. Chem. Phys.* **12** 10295–10312

Henze D K, Hakami A and Seinfeld J H 2007 Development of the adjoint of GEOS-Chem *Chem. Atmos. Chem. Phys.* **7** 2413–33

Henze D K, Seinfeld J H and Shindell D T 2009 Inverse modeling and mapping US air quality influences of inorganic $PM_{2.5}$precursor emissions using the adjoint of GEOS-Chem *Atmos. Chem. Phys.* **9** 5877–903

Hoesly R M, Smith S J, Feng L, Klimont Z, Janssens-Maenhout G, Pitkanen T and Zhang Q 2018 Historical (1750–2014) anthropogenic emissions of reactive gases and aerosols from the Community Emissions Data System (CEDS) *Geosci. Model Dev.* **11** 369–408

Holt J I, Solomon S and Selin N E 2017 Sensitivity of inorganic aerosol radiative effects to U.S. emissions *J. Geophys. Res.* **122** 6379–90

Huang X, Song Y, Li M, Li J, Huo Q, Cai X and Zhang H 2012 A high-resolution ammonia emission inventory in china *Global Biogeochem. Cycles* **26** GB1030

Janssens-Maenhout G, Crippa M, Guizzardi D, Dentener F, Muntean M, Pouliot G and Li M 2015 HTAP_v2.2: a mosaic of regional and global emission grid maps for 2008 and 2010 to study hemispheric transport of air pollution *Atmos. Chem. Phys.* **15** 11411–32

Kharol S K, Shephard M W, McLinden C A, Zhang L, Sioris C E, O'Brien J M and Krotkov N A 2018 Dry deposition of reactive nitrogen from satellite observations of ammonia and nitrogen dioxide overNorth America *Geophys. Res. Lett.* **45** 1157–66

Kille N, Baidar S, Handley P, Ortega I, Sinreich R, Cooper O R and Volkamer R 2017 The CU mobile Solar Occultation Flux instrument: structure functions and emission rates of NH_3, NO_2 and C_2H_6 *Atmos. Meas. Tech.* **10** 373–92

Krupa S 2003 Effects of atmospheric ammonia (NH_3) on terrestrial vegetation: a review *Environ. Pollut.* **124** 179–221

Li C, Martin R V, Shephard M W, Cady-Pereira K, Cooper M J, Kaiser J and Henze D K 2019 Assessing the Iterative Finite Difference Mass Balance and 4D-Var Methods to Derive Ammonia Emissions Over North America Using Synthetic Observations *J. Geophys. Res.* **124** 4222–36

Li Y, Schichtel B A, Walker J T, Schwede D B, Chen X, Lehmann C M and Collett J L 2016 Increasing importance of deposition of reduced nitrogen in theUnited States *Proc. Natl. Acad. Sci. U.S.A.* **113** 5874–9

Liu H, Jacob D J, Bey I and Yantosca R M 2001 Constraints from210Pb and7Be on wet deposition and transport in a global three-dimensional chemical tracer model driven by assimilated meteorological fields *J. Geophys. Res.* **106** 12109–28

Liu M, Huang X, Song Y, Xu T, Wang S, Wu Z and Zhu T 2018 Rapid SO_2 emission reductions significantly increase tropospheric ammonia concentrations over theNorth China Plain *Atmos. Chem. Phys.* **18** 17933–43

McQuilling A M and Adams P J 2015 Semi-empirical process-based models for ammonia emissions from beef, swine and poultry operations in theUnited States *Atmos. Environ.* **120** 127–36

Mikkelsen R *et al* 2009 Ammonia emissions from agricultural operations: fertilizer *Better Crops* **93** 9–11

Myhre G, Berglen T F, Johnsrud M, Hoyle C R, Berntsen T K, Christopher S A and Yttri K E 2009 Modelled radiative forcing of the direct aerosol effect with multi-observation evaluation *Atmos. Chem. Phys.* **9** 1365–92

Nah T, Guo H, Sullivan A P, Chen Y, Tanner D J, Nenes A and Weber R J 2018 Characterization of aerosol composition, aerosol acidity and organic acid partitioning at an agriculturally intensive rural southeastern US site *Atmos. Chem. Phys.* **18** 11471–91

Park R J, Jacob D J, Field B D, Yantosca R M and Chin M 2004 Natural and transboundary pollution influences on sulfate-nitrate-ammonium aerosols in the United States: Implications for policy *J. Geophys. Res.* **109** D15204

Paulot F, Jacob D J, Pinder R W, Bash J O, Travis K and Henze D K 2014 Ammonia emissions in theUnited States,European Union, and China derived by high-resolution inversion of ammonium wet deposition data: Interpretationwith a new agricultural emissions inventory (MASAGE_NH3) *J. Geophys. Res.* **119** 4343–64

Pinder R W, Adams P J and Pandis S N 2007 Ammonia emission controls as a cost-effective strategy for reducing atmospheric particulate matter in the eastern United States *Environ. Sci. Technol.* **41** 380–6

Pinder R W, Adams P J, Pandis S N and Gilliland A B 2006 Temporally resolved ammonia emission inventories:

Current estimates, evaluation tools and measurement needs *J. Geophys. Res.* **111** D16310

Russ A and Schaeffer E 2017. Ammonia emissions from broiler operations higher than previously thought. Environmental Integrity Project (https://www.environmentalintegrity.org/wp-content/uploads/2017/12/Ammonia-Emissions.pdf)

Schiferl L D, Heald C L, Van Damme M, Clarisse L, Clerbaux C, Coheur P-F and Eilerman S J 2016 Interannual variability of ammonia concentrations over the United States: Sources and implications *Atmos. Chem. Phys.* **16** 12305–28

Shephard M W and Cady-Pereira K E 2015 Cross-track Infrared Sounder (CrIS) satellite observations of tropospheric ammonia *Atmos. Meas. Tech.* **8** 1323–36

Shephard M W, Cady-Pereira K E, Luo M, Henze D K, Pinder R W, Walker J T and Clarisse L 2011 TES ammonia retrieval strategy and global observations of the spatial and seasonal variability of ammonia *Atmos. Chem. Phys.* **11** 10743–63

Shephard M W, Dammers E, Cady-Pereira K E, Kharol S K, Thompson J, Gainariu-Matz Y and Zheng Q 2020 Ammonia measurements from space with the Cross-track Infrared Sounder (CrIS): Characteristics and applications *Atmos. Chem. Phys* **20** 2277–302

Sutton M A, Howard C M, Erisman W, Billen G, Bleeker A, Grennfelt P and Grizzetti B 2011 *The European Nitrogen Assessment: Sources, Effects and Policy Perspectives* (Cambridge: Cambridge University Press)

Tobin D 2012. Early Checkout of the Cross-track Infrared Sounder (CrIS) on Suomi-NPP, Through the Atmosphere, Summer 2012

U.S. EPA 2018 Data from the 2014 National Emissions Inventory Version 2

United States Department of Agriculture 2014 Ammonia emissions: What to know before you regulate Task Force Accomplishments and Recommendations (https://www.nrcs.usda.gov/wps/PA_NRCSConsumption/download?cid=stelprdb1268626&ext=pdf)

Van Damme M, Clarisse L, Heald C L, Hurtmans D, Ngadi Y, Clerbaux C and Coheur P F 2014 Global distributions, time series and error characterization of atmospheric ammonia (NH_3) from IASI satellite observations *Atmos. Chem. Phys.* **14** 2905–22

Van Damme M, Clarisse L, Whitburn S, Hadji-Lazaro J, Hurtmans D, Clerbaux C and Coheur P-F 2018 Industrial and agricultural ammonia point sources exposed *Nature* **564** 99

Wang Q, Jacob D J, Fisher J A, Mao J, Leibensperger E M, Carouge C C and Doherty S J 2011 Sources of carbonaceous aerosols and deposited black carbon in theArctic in winter-spring: Implicationsfor radiative forcing *Atmos. Chem. Phys.* **11** 12453–73

Wang Y, Jacob D J and Logan J A 1998 Global simulation of tropospheric O_3-NO_x-hydrocarbon chemistry: 1. Model formulation *J. Geophys. Res.* **103** 10713–25

Warner J X, Dickerson R R, Wei Z, Strow L L, Wang Y and Liang Q 2017 Increased atmospheric ammonia over the world's major agricultural areas detected from space *Geophys. Res. Lett.* **44** 2875–84

Warner J X, Wei Z, Strow L L, Dickerson R R and Nowak J B 2016 global tropospheric ammonia distribution as seen in the 13-year AIRS measurement record *Atmos. Chem. Phys.* **16** 5467–79

Wesely M 1989 Parameterization of surface resistances to gaseous dry deposition in regional-scale numerical models *Atmos. Environ.* **23** 1293–304

Wu Y, Gu B, Erisman J W, Reis S, Fang Y, Lu X and Zhang X 2016 $PM_{2.5}$ pollution is substantially affected by ammonia emissions in China *Environ. Pollut.* **218** 86–94

Yu F, Nair A A and Luo G 2018 Long-term trend of gaseous ammonia over the United States: Modeling and comparison with observations *J. Geophys. Res.* **123** 8315–25

Zavyalov V, Esplin M, Scott D, Esplin B, Bingham G, Hoffman E and Phillips L 2013 Noise performance of the CrIS instrument *J. Geophys. Res.* **118** 13,108–13,120

Zhang L, Chen Y, Zhao Y, Henze D K, Zhu L, Song Y and Huang B 2018 Agricultural ammonia emissions in China: Reconciling bottom-up and top-down estimates *Atmos. Chem. Phys.* **18** 339–55

Zhang L, Gong S, Padro J and Barrie L 2001 A size-segregated particle dry deposition scheme for an atmospheric aerosol module *Atmos. Environ.* **35** 549–60

Zhang L, Jacob D J, Knipping E M, Kumar N, Munger J W, Carouge C C and Chen D 2012 Nitrogen deposition to the United States: Distribution, sources and processes *Atmos. Chem. Phys.* **12** 4539–54

Zhu L, Henze D K, Bash J O, Cady-Pereira K E, Shephard M W, Luo M and Capps S L 2015 Sources and impacts of atmospheric NH_3: Current understanding and frontiers for modeling, measurements and remote sensing in North America *Curr. Pollut. Rep.* **1** 95–116

Zhu L, Henze D K, Cady-Pereira K E, Shephard M W, Luo M, Pinder R W and Jeong G-R 2013 Constraining U.S. ammonia emissions using TES remote sensing observations and the GEOS-Chem adjoint model *J. Geophys. Res.* **118** 3355–68